The effect of tensile and compressive loading on the hierarchical strength of idealized tropocollagen–hydroxyapatite biomaterials as a function of the chemical environment

2009 J. Phys.: Condens. Matter 21 205103

(http://iopscience.iop.org/0953-8984/21/20/205103)

IOP Publishing Journal of Physics: Condensed Matter

J. Phys.: Condens. Matter **21** (2009) 205103 (13pp) doi:10.1088/0953-8984/21/20/205103

The effect of tensile and compressive loading on the hierarchical strength of idealized tropocollagen–hydroxyapatite biomaterials as a function of the chemical environment

Devendra K Dubey and Vikas Tomar[1]

Aerospace and Mechanical Engineering, University of Notre Dame, IN 46556, USA

E-mail: vikas.tomar@nd.edu

Received 18 November 2008, in final form 12 March 2009
Published 8 April 2009
Online at stacks.iop.org/JPhysCM/21/205103

Abstract

Hard biomaterials such as bone, dentin and nacre have primarily a polypeptide phase (e.g. tropocollagen (TC)) and a mineral phase (e.g. hydroxyapatite (HAP) or aragonite) arranged in a staggered manner. It has been observed that the mechanical behaviour of such materials changes with the chemical environment and the direction of applied loading. In the presented investigation, explicit three-dimensional molecular dynamics (MD) simulations based analyses are performed on idealized TC–HAP composite biomaterial systems to understand the effects of tensile and compressive loadings in three different chemical environments: (1) unsolvated, (2) solvated with water and (3) calcinated and solvated with water. The MD analyses are performed on two interfacial supercells corresponding to the lowest structural level (level n) of TC–HAP interactions and on two other supercells with HAP supercells arranged in a staggered manner (level $n + 1$) in a TC matrix. The supercells at level $n + 1$ are formed by arranging level n interfacial supercells in a staggered manner. Analyses show that at level n, the presence of water molecules results in greater stability of TC molecules and TC–HAP interfaces during mechanical deformation. In addition, water also acts as a lubricant between adjacent TC molecules. Under the application of shear stress dominated loading, water molecules act to strengthen the TC–HAP interfacial strength in a manner similar to the action of glue. An overall effect of the observed mechanisms is that, in a staggered arrangement, tensile strength increases in the presence of water and calcinated water environments. On the other hand, corresponding compressive strength decreases under similar circumstances. Fundamentally, supercells with primarily normal load transfer at the TC–HAP interfaces are stronger in tensile shear loading. On the other hand, supercells with primarily tangential or shear load transfer at the TC–HAP interfaces are stronger in compressive shear loading. A combination of changes in chemical environment from vacuum to calcinated water and changes in interfacial configurations in a staggered arrangement could be chosen to make the TC–HAP material stronger under applied deformation.

(Some figures in this article are in colour only in the electronic version)

1. Introduction

Hard biological materials such as bone, dentin and nacre are a class of hierarchical nanocomposite material systems primarily consisting of a mineral phase (e.g. calcium hydroxyapatite (HAP), aragonite) and a polypeptides phase (e.g. tropocollagen (TC), chitin) in a staggered arrangement at the lowest fundamental length scale. In structural studies of such biological materials, it is observed that the mineral

[1] Author to whom any correspondence should be addressed.

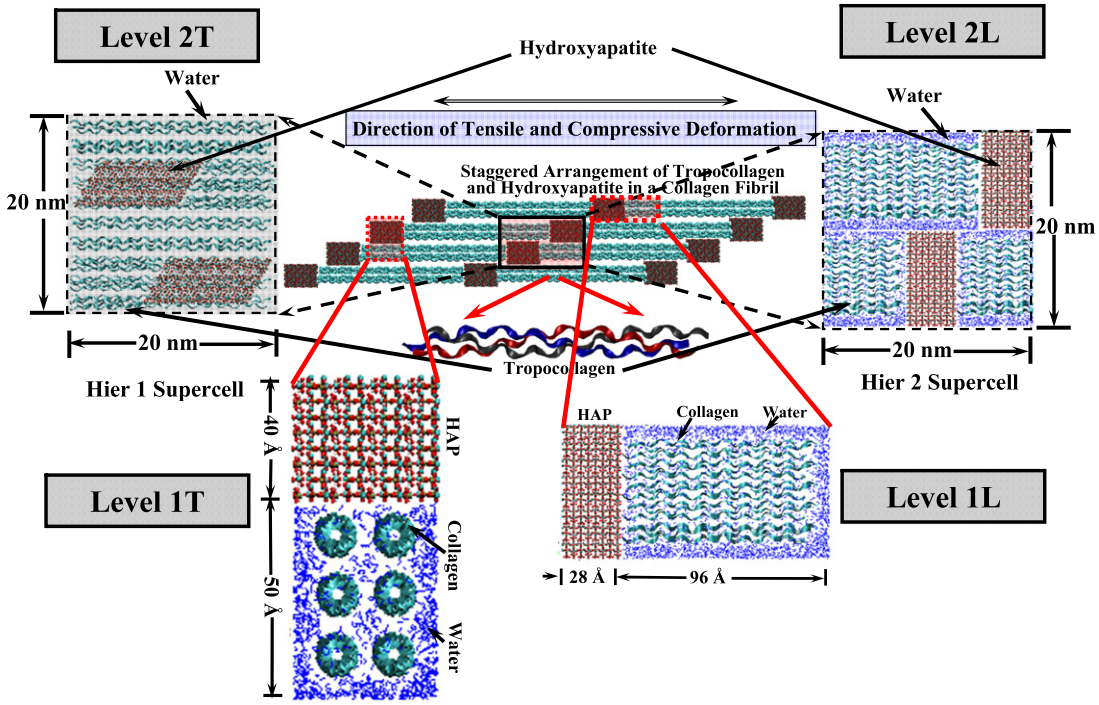

Figure 1. Schematic diagram showing the derivation of computational supercells from the staggered and layered assembly of TC molecules and HAP blocks to form a collagen fibril. Supercell Level 1L has TC molecules placed vertically on the HAP ⟨0001⟩ surface. Supercell Level 1T has TC molecules placed horizontally on the HAP ⟨0001⟩ surface. The Level 2L supercell is formed by combining different Level 1L supercells in a staggered manner. The Level 2T supercell is formed by combining different Level 1T supercells in a staggered manner.

crystals and the polypeptide molecules are arranged in a staggered fashion [1–4] (figure 1(a)). Additionally, it has been observed that the mechanical behaviour of such materials changes with chemical environment and the direction of applied loading [5–8]. In the presented research explicit three-dimensional molecular dynamics (MD) simulation-based analyses of tensile and compressive deformation in idealized TC–HAP composite biomaterial systems are reported to present an understanding of the effect of the chemical environment and loading directionality (tension versus compression) in three different chemical environments: (1) unsolvated (vacuum), (2) solvated (water) and (3) solvated in water with calcium ions (calcinated water). Such a TC–HAP combination is primarily found in bone tissue.

Experiments and modelling studies at the continuum scale have previously found a difference in tensile and compressive properties of bone tissue [9]. At the nanoscale, bone tissue primarily consists of a type-I collagen (TC) phase and a HAP phase ($Ca_5(PO_4)_3OH$). Despite the fact that TC is a soft phase and HAP is brittle, together they form a material of high mechanical strength and fracture toughness [10]. Bone consists of some other constituents as well (such as non-collagenous proteins, glycans, mineral impurities etc) [11]. However, interfacial interactions between the TC and the HAP phases along with their hierarchical arrangement are thought to be the most important factors imparting high strength and fracture toughness [12]. Figure 1 shows that a staggered arrangement is responsible for possible tension shear type load transfer between TC molecules and HAP crystals [13]. There have been explanations based on growth and mineralization for the existence of such an arrangement [2, 3, 14]. However, it may also be possible that the existence of such a structural arrangement is driven by its important role in imparting high mechanical strength.

With a view to understanding the role of TC molecules and HAP mineral, the mechanical behaviour of biological materials has previously been analysed using experiments, modelling and simulations. Experimental approaches have focused on analysing the tensile failure of single collagen fibres and fibrils [12, 15–17], and on analysing structural features at the nanoscale and its relation with the bone tissue failure [18–20]. Modelling using the continuum approaches has focused on understanding the role played by the shear strength of TC molecules and the tensile strength of HAP mineral in the fault tolerant hierarchical structural design of biomaterials [5, 10, 13, 21]. Explicit simulations using MD schemes have focused on understanding the mechanical behaviour and properties of TC molecules in different structural configurations [22–24], on understanding hierarchical organization of TC molecules into collagen fibrils and its effect on mechanical properties [25, 26], on understanding properties of hydrated TC molecules [27, 28], and on understanding the stability of the TC molecule with respect to changes in residue sequences [29]. However, MD based analyses of the effects of different interfacial arrangements and the effects of the staggered arrangement of TC and HAP on mechanical strength under tensile and compressive loading have not been performed. Such analyses could reveal important evidence about the role of interfacial arrangement, loading directionality, structural hierarchy and

chemical environment in biomaterial failure. The present work reports such analyses.

In the presented research we analyse four different supercells of TC and HAP as shown in figure 1. Two interfacial supercells corresponding to the lowest fundamental length scale are referred to as Level 1L and Level 1T. The Level 1L supercell has predominantly tensile load transfer between the TC–HAP interfaces. The Level 1T supercell has predominantly shear loading at the TC–HAP interfaces. Supercells at Levels $n + 1$, 2L and 2T, corresponding to the next level in the hierarchy $(n + 1)$ are formed by combining Levels 1L and 1T, respectively, in a staggered manner in a TC matrix. The choice of orientation of the HAP crystals in all supercells, the size of the supercells, and the number of supercells is limited due to the extensive computational time involved. Limitations of computational time is also the reason for the analyses in the presented work being performed only for an idealized TC–HAP composite biomaterial. The MD simulation results are compared with experiments as well as analysed using a well established tension shear chain (TSC) model for biomaterial failure characterization [5, 13].

2. Method and framework

The four different kinds of supercells generated are shown in figure 1: two interfacial supercells corresponding to the lowest structural level (level n: Levels 1L and 1T) of TC–HAP interactions and two other supercells with HAP supercells arranged in a staggered manner (level $n + 1$: Levels 2L and 2T) in a TC matrix. Levels 1L and 1T are two structurally distinct TC–HAP interfacial supercells (figure 1) such that Level 1L has TC molecules placed perpendicular to the HAP {0001} surface and Level 1T has TC molecules placed along the HAP {0001} surface. On the other hand, Level 2L has the HAP supercells embedded such that the {0001} surface of the HAP supercells is perpendicular to the longitudinal axes of TC molecules and Level 2T has the {0001} surface of the HAP supercells parallel to the longitudinal axes of TC molecules. The HAP {0001} surface is chosen because this surface is the most energetically stable surface of HAP crystals [30], permitting us to analyse the effect of the interfacial arrangement in detail without the effect of factors such as surface reconstruction of the HAP surface etc. The Level 1L and Level 1T supercells are generated based on information about the two possible distinct types of load transfer mechanism: (1) pure tensile loading and (2) pure shear loading. The size of the Level 1L and 1T supercells was chosen as the maximum size which could be computationally analysed using 3D MD in a period of at most 7–10 days. The size of Levels 2L and 2T was chosen such that HAP supercells in these levels could be of the same approximate dimensions as in the case of Levels 1L and 1T while forming a staggered arrangement subjected to 3D periodic boundary conditions (PBC). The number of supercells and the choice of orientation of the HAP crystals in all supercells are limited by the computational cost. All supercells are analysed for uniaxial deformation using a well established method [31] in three different chemical environments: (1) vacuum, (2) water and (3) calcinated water. For the supercells of Levels 2L and 2T, the computational cost of deformation analyses is very high (of the order of 15–20 days per analysis). In addition, we did not find any significant difference between the longitudinal and transverse stretching results. Therefore, the analyses here present longitudinal stretching results for Levels 2L and 2T. In the case of the Level 1L and 1T supercells, the computational cost was lower (of the order of 7–10 days per analysis).

The structure of a full length TC molecule is a triple helix of three polypeptide chains (two alike alpha chains, and one beta chain). Each chain comprises approximately a thousand amino acids (residues) with the characteristic Gly–X–Y triplet sequence (Gly is glycine and X, Y can be any other amino acid). The residue sequence of the full length TC molecule in our study is acquired from reference [32] (PDB ID '1YGV'). This residue sequence information is used to generate the atomic level structure of the TC molecule using the gencollagen package [33], and hydrogen atoms are added by the psfgen module of the NAMD package [34] for performing MD simulations. The TC molecule used in the supercells consists of 90 residues, and is obtained by severing the first 30 residues from each polypeptide chain, starting from the C-terminal of the full length TC molecule with strict Gly–X–Y sequence (required for gencollagen). The HAP supercell is generated by using fractional coordinate and unit cell parameter information provided by Elliott *et al* [35] for monoclinic phase of HAP with space group $P2_1/b$, $a = 9.4214$ Å, $b = 2a$, $c = 6.8814$ Å, and $\gamma = 120°$. The HAP supercell consists of 64 unit cells (four unit cells along all three crystallographic axes) with 88 atoms per unit cell and one TC molecule of 90 residues consists of 1135 atoms.

2.1. Force field functions and parameters

All simulations are performed using the NAMD package as it works better with large biomolecules and can be scaled well to very large processor counts [36]. A combination of the CHARMM22 force field [37] and an inorganic force field reported earlier for HAP [38, 39], is used to model the atomistic interactions. The interfacial interactions between the TC and the HAP phases are described based on quantum mechanically derived van der Waals parameters available in the CHARMM22 force field. The CHARMM22 potential energy function [40] is composed of an intra-atomic term, E_{INTRA}, and an inter-atomic term, E_{INTER},

$$E = E_{\mathrm{INTRA}} + E_{\mathrm{INTER}}. \tag{1}$$

The term E_{INTRA} is given by,

$$\begin{aligned} E_{\mathrm{INTRA}} = {} & \sum k_{\mathrm{b}}(r_{ij} - r_o)^2 + \sum k_\theta(\theta_{ijk} - \theta_o)^2 \\ & + \sum k_{\mathrm{UB}}(r_{ik} - r'_o)^2 + \sum |k_\phi| - k_\phi \cos(n\phi) \\ & + \sum k_\omega(\omega - \omega_o)^2. \end{aligned} \tag{2}$$

Here, k_{b}, k_θ, k_{UB}, k_ω and k_ϕ are force constants, r_o, θ_o, r'_o and ω_o are the equilibrium bond length between sites i and j, the equilibrium bond angle, the equilibrium bond length between sites i and k, and the equilibrium improper torsion angle, respectively, $r_{i,j}$ is the distance between sites i and j,

$r_{i,k}$ is the distance between sites i and k, θ_{ijk} is bond angle between sites i, j and k, and ϕ and ω are the dihedral angle and improper torsion angle, respectively. The third term in equation (2) denotes the Urey–Bradley term. The inter-atomic term includes Coulombic and Lennard-Jones potential terms and is given by

$$E_{\text{INTER}} = \sum \frac{1}{4\pi\varepsilon_o}\frac{q_i q_j}{r_{i,j}} + \sum \varepsilon_{ij}\left[\left(\frac{R_{\min,i,j}}{r_{i,j}}\right)^{12} - 2\left(\frac{R_{\min,i,j}}{r_{i,j}}\right)^{6}\right]. \quad (3)$$

Here, $r_{i,j}$ is the distance between the ith and jth particles with charges q_i and q_j and ε_o is the vacuum dielectric constant. The terms ε_{ij} and $R_{\min,i,j}$ determine the minimum and zero of the van der Waals term. The particle mesh Ewald method is used to calculate electrostatic interactions with a cut-off of 12 Å. The CHARMM22 force field and topology parameters for the TC molecule are directly obtained from the CHARMM website [40]. For water, we employed the TIP3 model [41]. Proline frequently occupies the X and Y positions in the Gly–X–Y triplet and some of them hydroxylate to hydroxyproline (HYP), which has been reported to enhance the stability of the TC triple helix [42–45]. Parameters for the non-standard residue HYP are obtained using the procedure outlined by Anderson [46].

2.2. Simulation details

Simulations are performed with PBCs imposed in the three dimensions. In order to create water and calcinated water environments, water molecules and calcium ions are added to the supercells using the 'SOLVATE' module in visual molecular dynamics (VMD) software. This approach of adding solvating molecules is a standard approach followed in biomolecular simulations [47, 48]. Care is taken such that charge neutrality exists in all scenarios. For all supercells, energy minimization is first performed using conjugate gradient and line search algorithms, until there is no significant change in the total energy. After minimization, MD equilibration with a time-step of 1 fs/step is performed at 0% strain in two different ensembles: (1) isothermal–isobaric (NPT) ensemble for equilibration at 1 atm pressure and 300 K temperature until the volume of the supercell being equilibrated has stabilized and there are minimal pressure fluctuations; and (2) canonical (NVT) ensemble for equilibration at 300 K until the fluctuations in the temperature subside. The termination criterion for equilibration is: when there is no significant change in the supercell volume and a mean pressure of 1 atm with mean temperature of 300 K is achieved. During NPT equilibration, a flexible cell flag is used to allow cell dimensions to change independently in three orthogonal directions and the resulting equilibrated structure is then used for the deformation study in the NVT ensemble.

The stress–strain curve information is generated based on the well established procedure of Tomar and Zhou [31]. In order to obtain stress–strain plots for a supercell such as Inter1L, first the virial stress tensor for the supercell at 0% strain is recorded. Then, a strain increment of $\varepsilon = 2\%$ for tension and $\varepsilon = -2\%$ for compression is given to the supercell in the designated stretching or compression direction. In order to account for Poisson's effect, the cell is compressed or stretched by $\nu\varepsilon\%$ for tension and compression, respectively. Here, ν is Poisson's ratio taken to be 0.3 based on an average of the reported literature values for TC and HAP. The cell is then equilibrated using the same sequence of NPT–NVT equilibration as that at 0%. The virial stress tensor at the end of the equilibration is recorded as the stress tensor corresponding to the strain level of 2%. Subsequently, the cells are further subjected to straining of ±2%, depending upon whether its tension or compression and the virial stress recorded after equilibration at the resulting strain level. Equilibrated structure from one simulation is used as an input structure for the next successive deformation level. This cycle continues until a strain level of 20% is reached. The values at 0% are considered residual stress values and subtracted from stress values at all strain levels so that the initial 0% deformed state corresponds to the unstressed state.

3. Results and analyses

The analyses focus on understanding the correlations among the peak stress, the relative arrangement of TC molecules with respect to the HAP mineral, the direction of loading, and the chemical environment. It is important to understand at this point that the simulations are classical in nature and, therefore, analyses do not focus on the fundamental bond breaking mechanisms at the localized length scale of individual bonds. Accordingly, the insights offered by the analyses mainly focus on an overall mechanistic understanding without providing details about the mechanisms of individual bond breaking.

3.1. Mechanism of deformation and failure

During analyses it was invariably found that the dominant tensile failure mechanism is the separation of TC–HAP interfaces. The compressive failure mechanism is found to be primarily driven by shear stress. The peak of the compression stress–strain curves was found to coincide with shear breakage of mineral crystals in each case. Figure 2 shows a snapshot explaining tensile interfacial failure for supercell Level 2T. At the peak of the tensile stress–strain curve in all environments, it is observed that TC molecules start cleaving off the HAP surface. After the peak stress point has passed, the ends of the TC molecules detach from the HAP surface and start folding back on to the TC molecules. At physiological pH values the amino acids in TC molecules are for the most part zwitterionic with NH_3^+ and COO^- groups. These groups are strongly attracted to the ions in the HAP surface (Ca^{2+}, PO_4^{3-} and OH^-), Posner and Beebe [49]. Since TC is a flexible chain-like molecule it elongates on applied deformation but cleaves off after the point when it is fully stretched. Such cleavage results in local nanoscale interfacial failure. We observed that in almost all cases the failure occurs in a ductile fashion. Accordingly, the effective strength of the supercells under study needs to be characterized using a measure based on principal stresses that can effectively describe ductile material

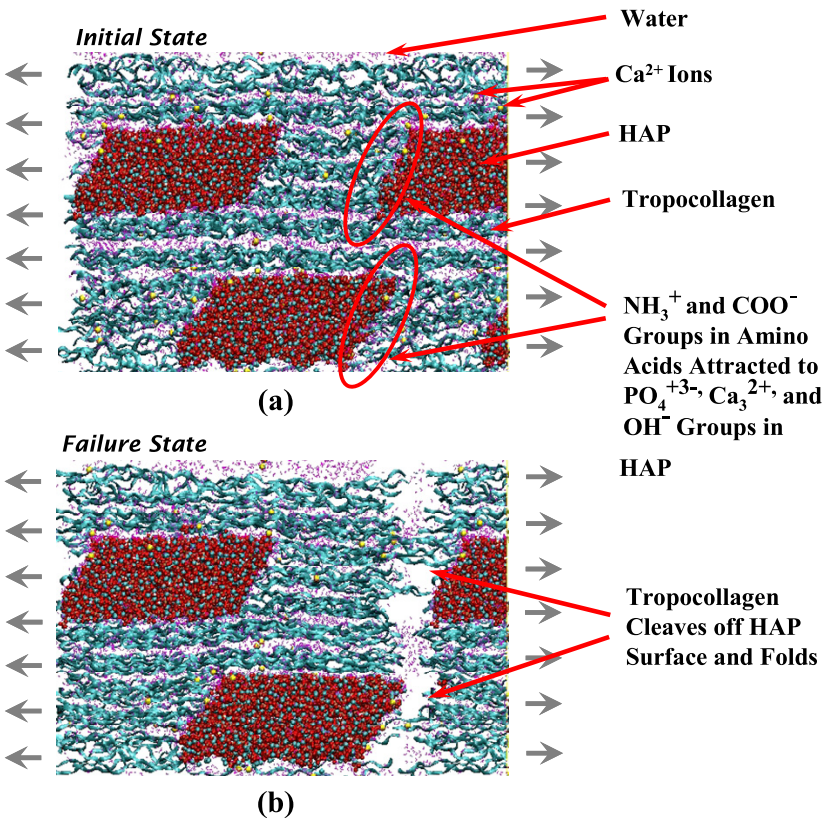

Figure 2. (a), (b) Snapshots showing the two primary stages of deformation in the Level 2T supercell. Almost invariably the peak of the stress–strain curves coincides with the collagen cleaving from the HAP–TC interface. Similarly, a cleavage-driven interfacial separation mechanism was observed for Levels 1L, 1T and 2L as well.

failure. We chose the widely accepted von Mises stress as such a measure.

We performed extensive visual analyses of the tensile and compressive deformation to understand the role of the changing chemical environment on the changes in the mechanical behaviour of TC and HAP (figure 3). We observed that the water molecules act as a lubricant between adjacent TC molecules during axial stretching when the loading is dominantly tensile. However, under dominant shear type loading the water molecules act as glue between adjacent TC molecules and at the TC–HAP interfaces, increasing the bond strength. Overall, in all cases, we saw that the presence of calcinated or non-calcinated water molecules results in a significant stability of TC molecules. At the TC–HAP interfaces the presence of water molecules results in increased interfacial bond strength through electrostatic bridging. This increase is substantial for tensile and tension shear loading where TC molecules have very low or no opportunity for folding onto themselves. These mechanistic insights are in accordance with the earlier findings of Zhang *et al* [28]. The further analyses in this paper are presented in light of these mechanistic findings.

3.2. Effect of chemical environment

In animal bodies biological materials are surrounded by various bodily fluids, with water and salts being the main component of the fluids. It is thought that the presence of water and Ca^{2+} ions affects the mechanical properties of collagenous tissues [19, 50]. To understand this issue the supercell deformation is analysed in vacuum, water and calcinated water environments. Figure 4 shows the tensile and compressive stress–strain curves obtained for Level 1L and 1T supercells in all chemical environments. In the case of the Level 1L supercell, tensile loading is shared by TC, HAP and the TC–HAP interface. However, during compression most of the applied compressive strain is transferred to the folding of TC molecules and a relatively small amount is transferred to the HAP block through the TC–HAP interface. This explains that the observed compressive strength of Level 1L supercells is significantly less than the tensile strength. The change in the chemical environment has more impact on the tensile than compressive strength of Level 1L. This is explained by the observation that both during tension and compression, the interfacial bond strengthening due to the change in chemical environment (explained in section 3.1) affects the extent of load transfer between the HAP and the TC at TC–HAP interfaces. The interfacial strengthening has no direct role to play in the compressive deformation and hence has little impact. In the case of the Level 1T supercell, tensile loading is also shared by TC, HAP and the TC–HAP interface with one significant difference now when compared to Level 1L. While in the case of the Level 1L supercell TC–HAP interfacial interactions involved normal (perpendicular) load transfer, in Level 1T the

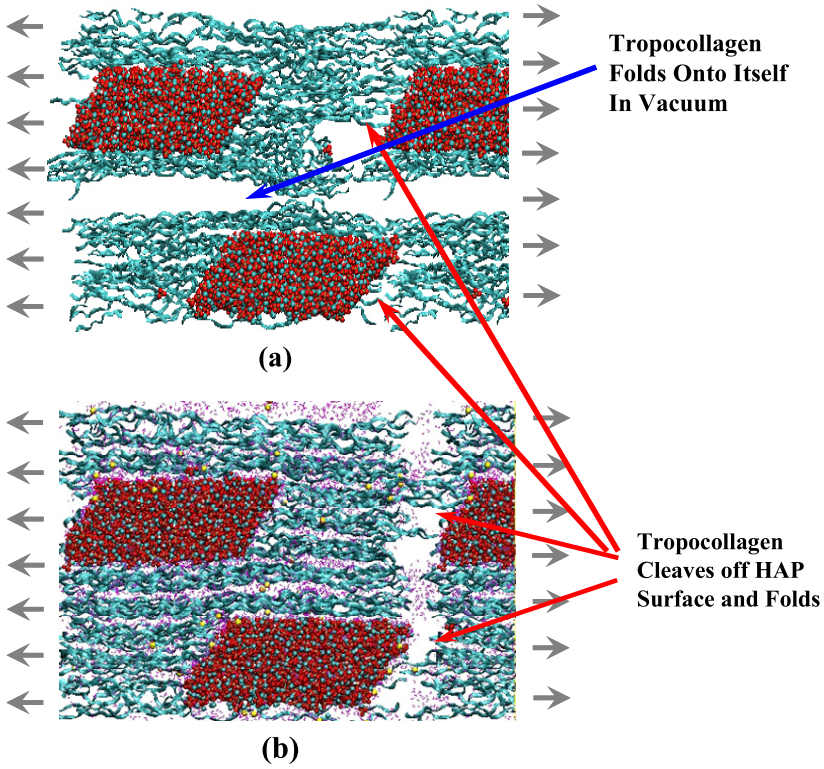

Figure 3. Snapshots comparing Level 2T supercell failure under tension in (a) vacuum and (b) water environments. In the vacuum besides interfacial failure as observed earlier in figure 2 we also observe a folding of TC molecules onto themselves, indicating that TC molecules may not have a stable structure in the absence of water molecules.

load transfer at the TC–HAP interface occurs through shearing between the TC and the HAP phases. In addition, contrary to the case of Level 1L, the mechanism of load transfer does not change when the loading direction changes from tension to compression. Correspondingly, we observe no tension–compression strength asymmetry in a vacuum environment for Level 1T. Contrary to what is observed in the case of Level 1L, we observe that the environment affects the tensile as well as the compressive strengths significantly. Unlike the case of Level 1L, in Level 1T a significant portion of applied tensile and compressive deformation is shared by the TC–HAP interface. Consequently, increase in the interfacial strength with change in the chemical environment (explained earlier) directly results in significant strengthening of the material.

Figure 5 shows the stress–strain curves under tension and compression for Level 2L and 2T supercells. As shown in the figure, strength values for hierarchical supercells (Levels 2L and 2T) are an order of magnitude less than those for interfacial supercells (Levels 1L and 1T). Level 2 supercells are formed by embedding Level 1 supercells in a TC matrix. Dominant tensile loading at the TC–HAP interfaces and in HAP in the case of supercell Level 1L and dominant shear loading at the TC–HAP interfaces in the case of supercell Level 1T is replaced by a combination of tensile and shear loading. In the case of the Level 2L supercell tensile loading results in stretching of TC, HAP and TC–HAP interfaces with shear load based transfer of stresses between adjacent HAP blocks through the TC matrix. During compression, however, the majority of applied strain in Level 2L gets allocated to the folding of the TC matrix with a small share going to the compression of HAP blocks through TC–HAP interfacial interactions. Correspondingly, there is significant tension–compression strength asymmetry in the case of the Level 2L supercell. Contrary to what was observed in the case of the Level 1L supercell, we observe a significant effect of the change in the chemical environment for the Level 2L supercell. The reason for this is similar to what was explained for Levels 1L and 1T. In this case we have combined shear tension load transfer at the TC–HAP interfaces. In addition, as explained earlier, water acts as a lubricant between adjacent TC molecules in addition to stabilizing TC intermolecular interactions. A combined effect of these factors is that under tension, Level 2L has better mechanical strength. TC molecules are, however, unable to resist compression. Therefore, the TC–HAP interface has little role to play in determining the compressive strength (since it is strain controlled deformation). Since water acts as a lubricant between adjacent TC molecules, the change in chemical environment from vacuum to water and calcinated water leads to a reduction in compressive strength. The Level 2T supercell is formed by putting Level 1T supercells in a TC matrix in a staggered manner. Accordingly, shear deformation at the TC–HAP interfaces is the primary mechanism of load transfer. However, by virtue of the TC matrix the load distribution mechanism is a combination of tensile and shear deformations. Owing to the shear dominance at the TC–HAP interfaces, the change in chemical environment increases the system's strength under tension. Level 2T is the strongest system under tension. However, under compression, due to

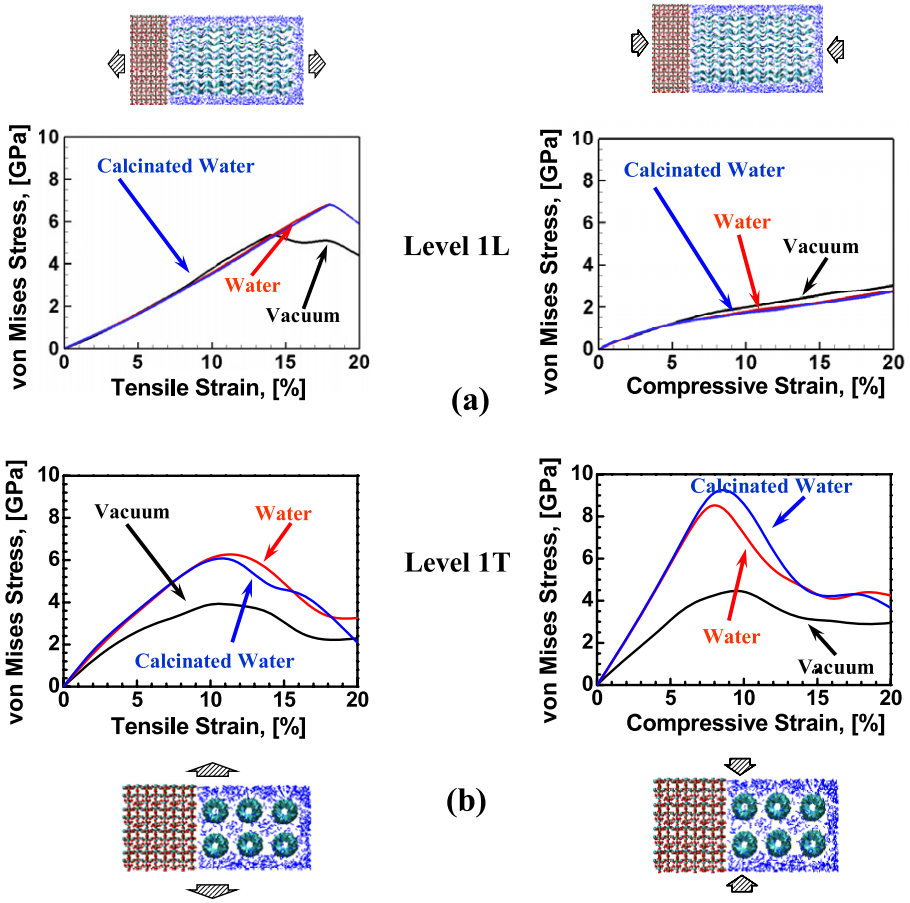

Figure 4. Tensile and compressive von Mises stress versus strain plots as a function of the chemical environment in the case of (a) a Level 1L supercell loaded in the longitudinal direction and (b) a Level 1T supercell loaded in the transverse direction.

a similar mechanism observed in the case of Level 2L, the change in chemical environment results in a reduction in the mechanical strength of Level 2T. Overall, Level 2T is stronger than Level 2L owing to the dominance of shear interactions in the case of Level 2T. An interesting observation from figures 4 and 5 is that the introduction of hierarchy does not change the strain values corresponding to the peak stress in the stress–strain curve.

Figure 6 shows the peak stress and peak strain values corresponding to the stress–strain curves shown in figures 4 and 5, as a function of structural arrangement and chemical environment. As shown, the peak stress values for hierarchical supercells are an order of magnitude less than those for interfacial supercells, implying that the structural hierarchy results in a reduction of the strength and stiffness of the composites. This is clearly because Level 2 supercells have a significant amount of TC matrix. Peak stress values in the presence of water (water and calcinated water environments) consistently show an increase for all supercells. At level n, the highest increase is for the Level 1T supercell. At level $n+1$, however, the increase is of almost the same order for both supercells under tension and the decrease is of the same order under compression despite the different structural features, implying that the presence of TC matrix has a significant effect on material behaviour. The difference in peak stress values at level n is significantly higher than that at level $n+1$. Clearly, orientation has stronger effect at the smallest length scale. With the introduction of hierarchy, the effect of change in orientation on the change in strength diminishes.

Figure 7 shows a comparison of the values of Young's modulus for Level 1 (level n) and Level 2 (level $n+1$) supercells. Values of Young's modulus for hierarchical supercells are an order of magnitude less than those for interfacial supercells. At both levels of hierarchy, we see that Young's modulus of the supercell with a shear dominated deformation mechanism is higher. Figure 7 also shows the absolute upper and lower bounds of Young's modulus values for all supercells defined by the Voigt limit, E_{Voigt},

$$E_{\text{Voigt}} = E_{\text{m}}\phi_{\text{m}} + E_{\text{p}}\phi_{\text{p}}, \tag{4}$$

and the Reuss limit, E_{Reuss},

$$\frac{1}{E_{\text{Reuss}}} = \frac{1}{E_{\text{m}}\phi_{\text{m}}} + \frac{1}{E_{\text{p}}\phi_{\text{p}}}. \tag{5}$$

In the above equations, E_{m} and E_{p} are the values of Young's modulus for HAP mineral and TC molecules, respectively, in a vacuum, and ϕ_{m} and ϕ_{p} are the corresponding volume fractions. As shown, level n supercells have all modulus values within the bounds, while hierarchical

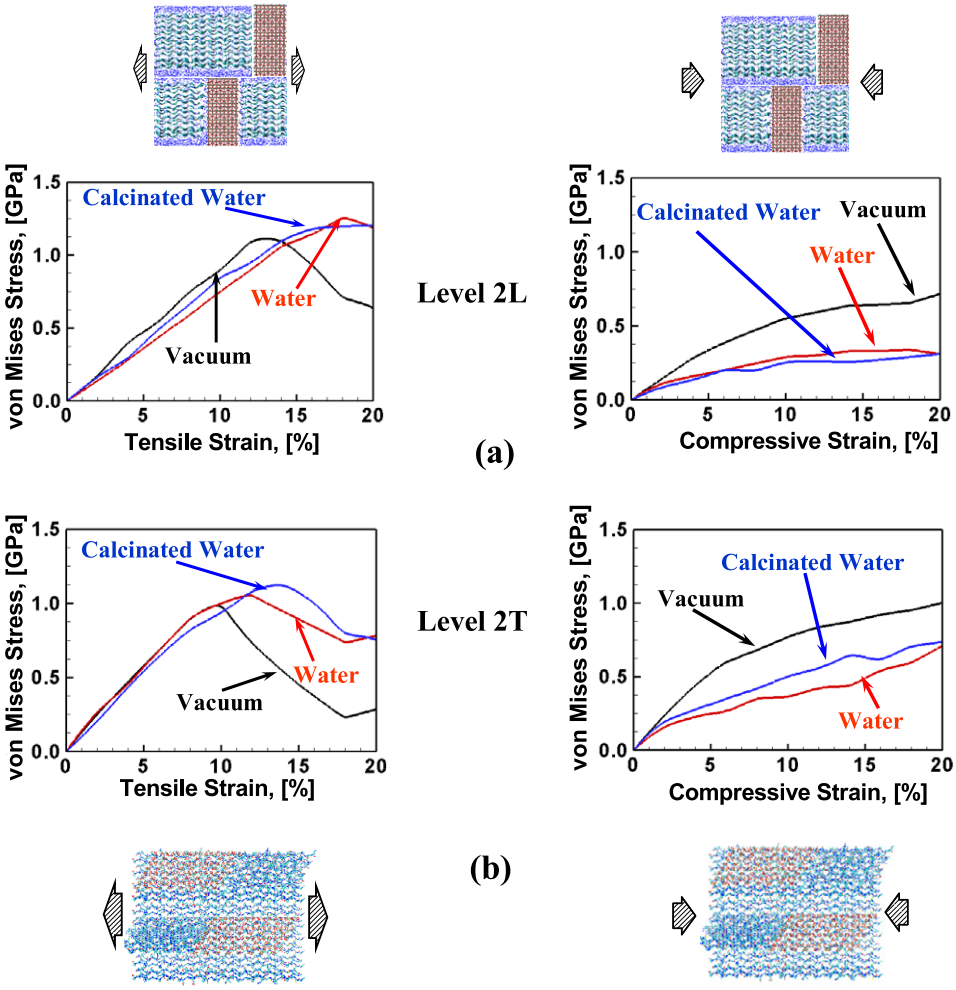

Figure 5. Tensile and compressive von Mises stress versus strain plots as a function of chemical environment in the case of (a) a Level 2L supercell loaded in the longitudinal direction and (b) a Level 2T supercell loaded in the longitudinal direction.

supercells (level $n + 1$) have almost all modulus values below the lower bound. It is important here to revisit the definition of Reuss and Voigt bounds. While the Reuss bound describes an extreme condition of iso-stress (stress being the same everywhere) in a sample, the Voigt bound describes a condition of iso-strain in a sample (strain being the same everywhere) [51]. An examination of individual component strains and stressed in Level 2 supercells showed that the conditions of iso-strain and iso-stress for uniformly applied external deformation do not apply to both the supercells. Earlier, Broedling *et al* [52] (see figure 12 in their paper) have also observed a similar violation of the Reuss limit for a staggered arranged Ni–Al composite at the lowest end of the length scale. An explanation of such observation has been offered by Chen *et al* [53]. According to them, it is possible that at high pressures, such as those observed in simulations here at the nanoscale (typical for a nanoscale MD simulation), a uniform transition from a state of iso-stress corresponding to the lower bound to a state of iso-strain corresponding to the higher bound may not be followed with changes in structural arrangement. In this condition it is possible that lower Reuss bound is violated. Such a condition is possible for materials with incipient plasticity [53] such as Level 2 supercells here consisting of polymer (TC) matrix.

Level 2 supercells represent the next level (level $n + 1$) in structural hierarchy to Level 1 type interfacial arrangements (level n) (figure 8). A well established TSC model for hierarchical nanocomposites correlates the strength and stiffness in materials with successive structural hierarchical levels [5]. Representations of the TSC model with an illustration of the two different levels of structural hierarchy are shown in figure 8. Under an applied load (shown by arrows), the HAP platelets carry most of the load while TC molecules transfer the load between HAP crystals via high shear zones at the HAP–TC interfaces. To correlate stiffness and strength values at different levels of hierarchy, the TSC model assumes a fractal hierarchy. Stiffness at the $(n + 1)$th level, E_{n+1}, is related to stiffness at nth level, E_n, by,

$$E_{n+1} = \phi_n E_n. \tag{6}$$

Under tension, the approximate volume fraction of the hard phase in the Level 2T supercell is $\phi_n \approx 0.25$. The average value of the Young's modulus from MD simulation for the Level 1T supercell, for all chemical environments, is

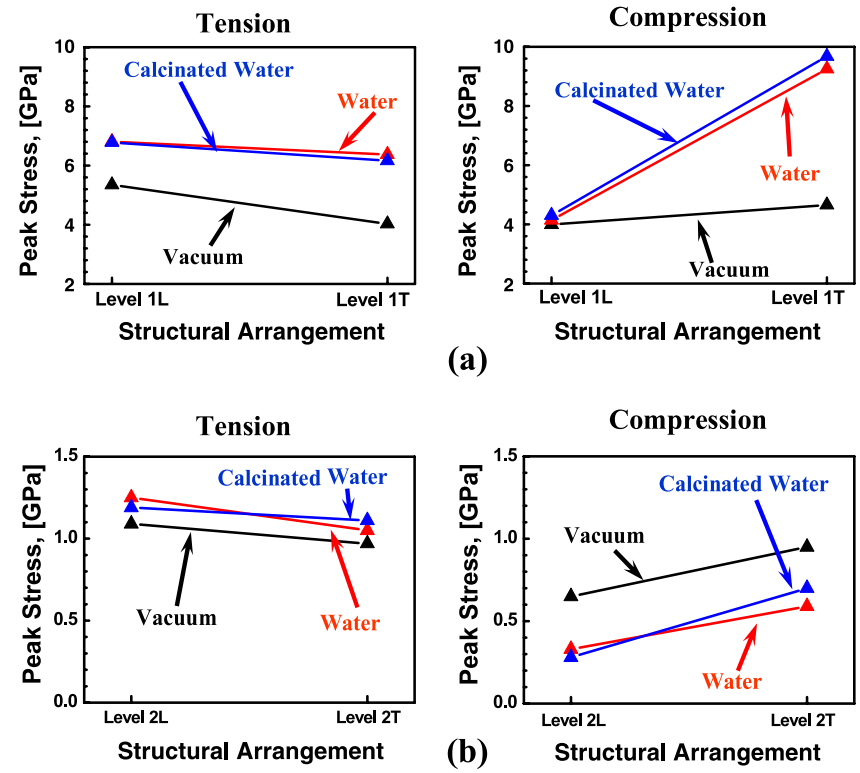

Figure 6. A comparison of the tensile and compressive peak stress values for (a) Level 1L and 1T supercells in vacuum, water and calcinated water atmospheres and (b) for Level 2L and 2T supercells in vacuum, water and calcinated water atmospheres.

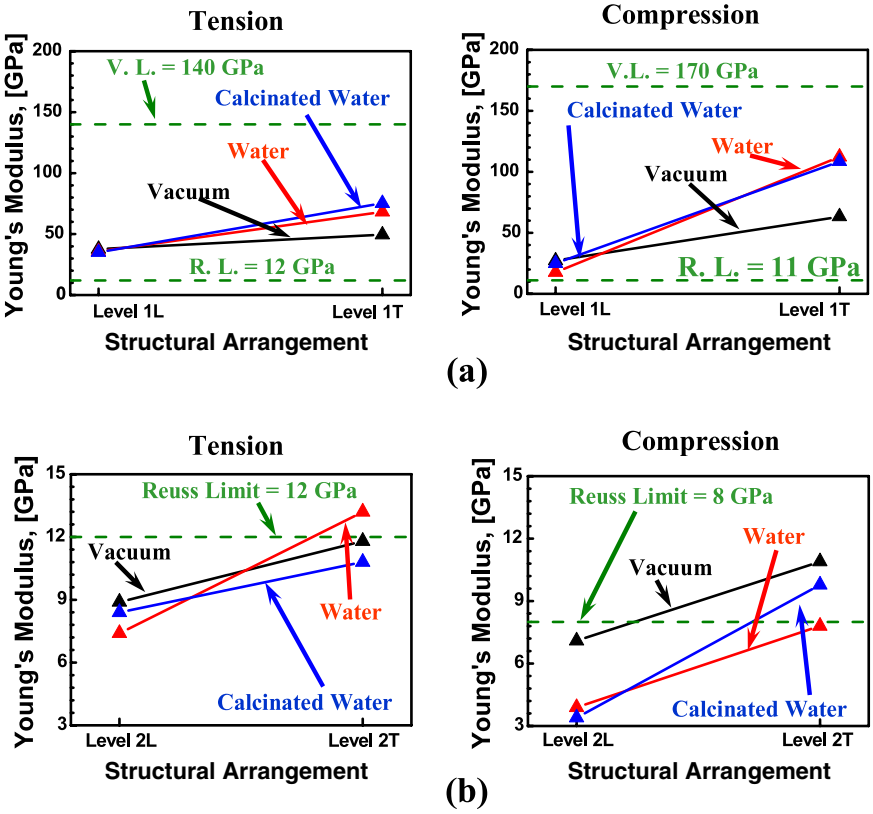

Figure 7. A comparison of the tensile and compressive Young's modulus values for (a) Level 1L and 1T supercells in vacuum, water and calcinated water atmospheres and (b) for Level 2L and 2T supercells in vacuum, water and calcinated water atmospheres.

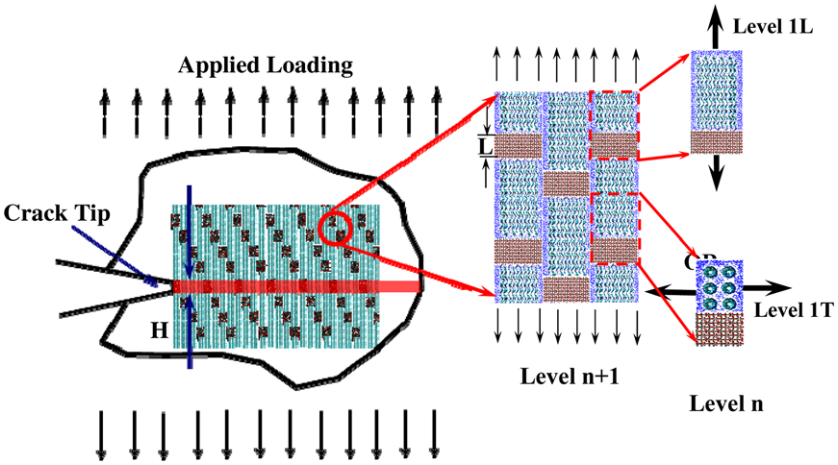

Figure 8. Schematic representation of a crack, the fracture localization zone, and the hierarchical levels in the tension shear chain model arrangement of HAP mineral platelets and TC molecules in a TC–HAP composite.

$E_n \approx 64.3$ GPa. Using equation (6), we get an average value of the modulus for the Level 2T supercell of $E_{n+1} \approx 16$ GPa. The value of Young's modulus for the Level 2L supercell obtained from MD simulation, averaged over all chemical environments, is ≈12 GPa, which is close to the calculated value of 16 GPa from the TSC model. Similarly, the approximate volume fraction of the hard phase present in the Level 2L supercell is $\phi_n \approx 0.5$. The value of Young's modulus from MD simulation for the Level 1L supercell, averaged over all chemical environments, is $E_n \approx 36$ GPa. Using equation (6), we get an average value of the modulus for the Level 2L supercell of $E_{n+1} \approx 18$ GPa. The average value of Young's modulus for the Level 2L supercell obtained from MD simulation, over all chemical environments, is ≈8 GPa. This analysis proves the applicability of an analytical model to the TSC results shown here. Encouraged by this analysis we apply the TSC model to analytically evaluate the interfacial strength of the supercells simulated.

3.3. Understanding the interfacial strength of the supercells based on the TSC model

The TSC model has been developed to describe the strength and fracture resistance of biomaterials consisting of a hard brittle phase such as HAP and a soft phase such as TC. At the most fundamental level, the model assumes that biomaterial failure occurs as a result of combined tensile and shear deformations. One of the important aspects of the TSC model is the prediction of the extent of peak fracture stress localization around the crack tip in a biocomposite such as the one shown in figure 8 [5, 13]. The extent of the fracture stress localization is predicted as a multiple of the length scale L shown in figure 8. Under an applied load (shown with arrows in figure 8) the HAP platelets carry most of the load while TC molecules transfer the load between HAP crystals via high shear zones at the HAP–TC interfaces. The width of the fracture localization zone, H, as a multiple of the characteristic length, L, of the TC–HAP arrangement is given as [13],

$$H = \xi L. \tag{7}$$

Here, ξ is a multiplying factor. In the present investigation, L is taken as the length of the mineral platelet. Since L is the same at both levels, n and $n+1$, the ξ values are an indicator of the extent of peak fracture stress localization and, thereby, an indicator of the fracture strength. Higher ξ implies that peak fracture stress is localized over a larger region resulting in higher fracture strength, as in the case of ductile materials. Lower ξ implies that the peak fracture stress is localized over smaller region resulting in lower fracture strength, as in the case of brittle materials. H is related to the fracture energy, J_c, by the integral over a crack tip contour,

$$J_c = H \int \sigma(\varepsilon)\, \mathrm{d}\varepsilon. \tag{8}$$

Here, σ and ε are the stress and effective strain of the supercell, respectively.

In order to study the interfacial strength, the above integral (equation (8)) is further simplified as [5, 13],

$$J_c = \frac{1}{8}\xi\phi_m L\frac{\tau_{int}^{*2}\rho^2}{E} + \xi(1-\phi_m)L\tau_{int}^{*}\varepsilon_p^f, \tag{9}$$

such that

$$\tau_{int}^{*} = \frac{\sigma_m^{*}}{\rho}. \tag{10}$$

In equations (9) and (10), τ_{int}^{*}, ρ, E, ε_p^f, ϕ_m and σ_m^{*} are interfacial shear strength, aspect ratio of mineral platelet, Young's modulus of the supercell, effective shear strain of protein before fracture, mineral volume fraction and maximum stress in the mineral platelet, respectively. Supercells at the levels n and $n+1$ have similar arrangement as the TSC model, with HAP crystals and TC molecules arranged in a staggered or layered fashion (figure 8). By using the TSC model equations, an effective length of the HAP crystals is first obtained, which is then used for further interfacial strength calculations. The length of HAP crystals in the supercells based on TSC model is towards the smaller side of the predicted range of values of length of HAP crystals in bone [54]. Young's modulus, ultimate strength and fracture

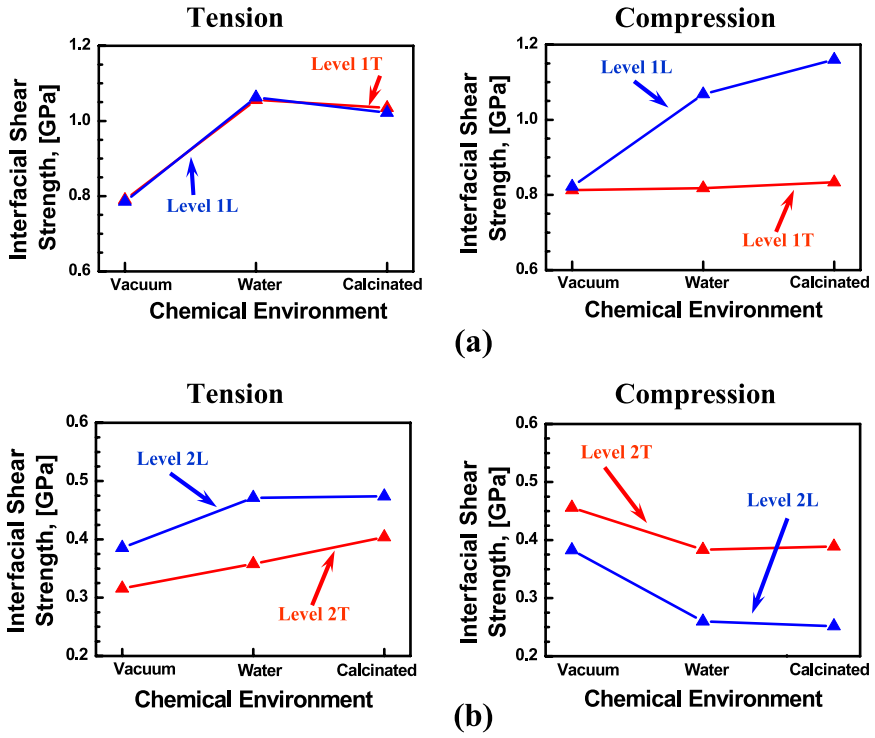

Figure 9. A comparison of the tensile and compressive interfacial strength values for (a) Level 1L and 1T supercells in vacuum, water and calcinated water atmospheres and (b) for Level 2L and 2T supercells in vacuum, water and calcinated water atmospheres.

energy values in equations (9)and (10) are substituted from stress–strain plots shown earlier.

The τ^*_{int} values obtained for the supercells at levels n and $n+1$ in vacuum, water and calcinated water environments are shown in figure 9. As shown, there is an order of two decrease in the τ^*_{int} values with increase in the level of hierarchy. Interfacial strength values corresponding to a particular level of hierarchy are of the same order. Change in the chemical environment from vacuum to calcinated water leads to an increase in the interfacial strength at level n. The effect of the change in the direction of loading on interfacial strength shows no clear trend at level n. However, at level $n+1$, changing the direction of loading shows a clear trend in the interfacial strength values as a function of direction of loading. At level $n+1$, interfacial strength increases with change in chemical atmosphere from vacuum to calcinated water. Since the Level 2L supercell has primarily normal load transfer at TC–HAP interfaces, it is stronger than the Level 2T supercell in tension. However, the reverse occurs under compression, where Level 2T supercell is stronger owing to the dominance of shear load transfer at the TC–HAP interfaces and folding of TC molecules in the case of Level 2L. We also see that changing the environment under compression causes strength to reduce, similar to what was reported earlier in stress–strain curves. Overall, the mechanical strength in the staggered arrangement is found to be strongly coupled to the texture in the TC–HAP arrangement and the directionality of loading. Fundamentally, supercells with primarily normal load transfer at the TC–HAP interfaces are stronger in tensile shear loading. On the other hand, supercells with primarily tangential or shear load transfer at the TC–HAP interfaces are stronger in compressive shear loading.

4. Discussion and conclusion

In the presented investigation, explicit three-dimensional MD simulation based analyses of tensile and compressive deformation in model TC–HAP systems are reported to gain an understanding of the effect of the nanoscale interfacial arrangement and structural hierarchy on biomaterial strength and its correlation with loading directionality. Some studies in the literature have pointed out that bone tissue at the nanoscopic length scales may be subjected to combined tensile and compressive loading while being subjected to a majority of compressive loading at the macroscopic length scale. It is therefore important to understand the effect of loading directionality on nanoscale interactions in bone tissue. Due to computational complexity, we have only considered two primary phases of bone tissue (TC and HAP). We are also limited in the length scale of our study due to computational time limitations. The analyses point to an important role for the coupling between loading directionality and structural arrangement in determining mechanical strength at the nanoscale.

Analysis results are based on our mechanistic understanding of the behaviour of TC and TC–HAP interfaces in different chemical atmospheres. In particular we found that water molecules act as a lubricant between adjacent TC molecules during axial stretching. The presence of water results in the quelling of non-equilibrium fluctuations in the TC molecules

leading to stable mechanical deformation (figure 3). These findings are supported through earlier analyses by Zhang *et al* [28]. In addition to the above findings we have also observed that the presence of water as well as calcinated water increases the strength of the TC–HAP interfaces though electrostatic bridging during tension as well as sliding. Previous studies have shown that hydration has a stabilizing effect on the collagen triple helix [55] and solvated TC molecules requires more energy to untie from the HAP surface [56]. The analyses confirmed that the presence of water indeed stabilizes the composite supercells and imparts a better mechanical performance for load handling. Water, being a polar solvent with the capability of making strong hydrogen bonds, has an affinity for the HAP surface [49] and TC molecules. As a result it acts as a bridge between the HAP surface and the TC molecules resulting in strengthening of the interface. Similar interaction behaviour of water at a protein–mineral interface is found in nacre as well [57]. Water also acts as glue between TC–TC interactions [28] and, thereby, delays the failure of the overall system.

The overall effect of these mechanistic findings is that under tension as well as under compression change in the interfacial strength causes changes in the mechanical strength of the systems. In addition to the changes in environment, change in the mechanical strength of the systems under study was also influenced strongly by the manner of load transfer at the TC–HAP interfaces. In particular, based on the system studies, two different types of load transfer mechanisms at the TC–HAP interfaces were possible: (1) shear transfer of load between TC and HAP at the TC–HAP interfaces; and (2) normal transfer of load between TC and HAP at the TC–HAP interfaces. TC molecules themselves are unable to resist transverse loads and can only resist tensile normal loads. Accordingly, the TC–HAP interfacial behaviour that changes with changing chemical environments dominates the material behaviour. The overall effect of these findings is that the mechanical strength in a staggered arrangement is strongly coupled to the texture in the TC–HAP arrangement and the directionality of loading. Fundamentally, supercells with primarily normal load transfer at the TC–HAP interfaces are stronger in tensile shear loading. On the other hand, supercells with primarily tangential or shear load transfer at the TC–HAP interfaces are stronger in compressive shear loading.

Analyses also revealed that failure of both interfacial and hierarchical supercells did not follow a scaling law and occurred in the peak strain value range of 10%–18%, regardless of an order of magnitude difference in the corresponding peak stress values. This result indicates that the failure of materials with staggered structure at the nanoscale may be characterized constitutively as strain driven rather than stress dominated. Currently, most of the bone biomaterials are characterized using constitutive theories that are strain based, e.g. Keaveny *et al* [58]. This result provided an argument for the extension of such theories to the nanoscale. An examination of scaling relations based on a very popular TSC model for supercells at levels n and $n + 1$ revealed that the predictions of the TSC model and MD simulations matched closely for all supercells in the case of Young's modulus values. The scaling relations indicated an order of magnitude reduction in the peak stress and Young's modulus values while scaling from levels n and $n + 1$. This result established the use of the TSC model at the nanoscale for biomaterials in real chemical environments.

References

[1] Weiner S, Talmon Y and Traub W 1983 Electron diffraction of mollusc shell organic matrices and their relationship to the mineral phase *Int. J. Biol. Macromol.* **5** 325–8

[2] Fratzl P, Fratzlzelman N, Klaushofer K, Vogl G and Koller K 1991 Nucleation and growth of mineral crystals in bone studied by small-angle x-ray scattering *Calcif. Tissue Int.* **48** 407–13

[3] Landis W J, Hodgens K J, Arena J, Song M J and McEwen B F 1996 Structural relations between collagen and mineral in bone as determined by high voltage electron microscopic tomography *Microsc. Res. Tech.* **33** 192–202

[4] Landis W J, Hodgens K J, Song M J, Arena J, Kiyonaga S, Marko M, Owen C and Mcewen B F 1996 Mineralization of collagen may occur on fibril surfaces: evidence from conventional and high-voltage electron microscopy and three-dimensional imaging *J. Struct. Biol.* **117** 24–35

[5] Gao H 2006 Application of fracture mechanics concepts to hierarchical biomechanics of bone and bone-like materials *Int. J. Fract.* **138** 101–37

[6] Fratzl P and Weinkamer R 2007 Nature's hierarchical materials *Prog. Mater. Sci.* **52** 1263–334

[7] Chen P-Y, Lin A Y M, Lin Y S, Seki Y, Stokes A G, Peyras J, Olevsky E A, Meyers M A and McKittrick J 2008 Structure and mechanical properties of selected biological materials *J. Mech. Behav. Biomed. Mater.* **1** 208–26

[8] Meyers M A, Chen P-Y, Lin A Y and Seki Y 2008 Biological materials: structure and mechanical properties *Prog. Mater. Sci.* **53** 1–206

[9] Mow V C and Huiskes R 2005 *Basic Orthopaedic Biomechanics & Mechano-Biology* (Baltimore, MD: Williams & Wilkins)

[10] Ji B and Gao H 2004 Mechanical properties of nanostructure of biological materials *J. Mech. Phys. Solids* **52** 1963–2000

[11] Weiner S and Wagner H D 1998 The material bone: structure mechanical function relations *Annu. Rev. Mater. Sci.* **28** 271–98

[12] Gupta H S, Wagermaier W, Zickler G A, Aroush D R-B, Funari S S, Roschger P, Wagner H D and Fratzl P 2005 Nanoscale deformation mechanisms in bone *Nano Lett.* **5** 2108–11

[13] Ji B H 2008 A study of the interface strength between protein and mineral in biological materials *J. Biomech.* **41** 259–66

[14] Wenk H R and Heidelbach F 1999 Crystal alignment of carbonated apatite in bone and calcified tendon: results from quantitative texture analysis *Bone* **24** 361–9

[15] Sasaki N and Odajima S 1996 Stress–strain curve and Young's modulus of a collagen molecule as determined by the x-ray diffraction technique *J. Biomech.* **29** 655–8

[16] Sasaki N and Odajima S 1996 Elongation mechanism of collagen fibrils and force–strain relations of tendon at each level of structural hierarchy *J. Biomech.* **29** 1131–6

[17] Eppell S J, Smith B N, Kahn H and Ballarini R 2005 Nano measurements with micro-devices: mechanical properties of hydrated collagen fibrils *J. R. Soc. Interface* **3** 117–21

[18] Hodge A J and Petruska J A 1963 Recent studies with the electron microscope on ordered aggregates of the tropocollagen macromolecule *Aspects of Protein Structure: Proceedings of a Symposium* ed G N Ramachandran (New York: Academic) pp 289–300

[19] Fantner G E, Hassenkam T, Kindt J H, Weaver J C, Birkedal H, Pechenik L, Cutroni J A, Cidade G A G, Stucky G D, Morse D E and Hansma P K 2005 Sacrificial bonds and hidden length dissipate energy as mineralized fibrils separate during bone fracture *Nat. Mater.* **4** 612–6

[20] Thurner P J, Erickson B, Jungmann R, Schriock Z, Weaver J C, Fantner G E, Schitter G, Morse D E and Hansma P K 2007 High-speed photography of compressed human trabecular bone correlates whitening to microscopic damage *Eng. Fract. Mech.* **74** 1928–41

[21] Jager I and Fratzl P 2000 Mineralized collagen fibrils: a mechanical model with a staggered arrangement of mineral particles *Biophys. J.* **79** 1737–46

[22] Lorenzo A C and Caffarena E R l 2005 Elastic properties, Young's modulus determination and structural stability of the tropocollagen molecule: a computational study by steered molecular dynamics *J. Biomech.* **38** 1527–33

[23] Buehler M J 2006 Nature designs tough collagen: explaining the nanostructure of collagen fibrils *Proc. Natl Acad. Sci. USA* **103** 12285–90

[24] Buehler M J 2007 Molecular nanomechanics of nascent bone: fibrillar toughening by mineralization *Nanotechnology* **18** 295102

[25] Israelowitz M, Rizvi S W H, Kramer J and Schroeder H P v 2005 Computational modeling of type I collagen fibers to determine the extracellular matrix structure of connective tissues *Protein Eng. Design Sel.* **18** 329–35

[26] Buehler M J 2008 Nanomechanics of collagen fibrils under varying cross-link densities: atomistic and continuum studies *J. Mech. Behav. Biomed. Mater.* **1** 59–67

[27] Handgraaf J W and Zerbetto F 2006 Molecular dynamics study of onset of water gelation around the collagen triple helix *Proteins: Struct. Funct. Bioinform.* **64** 711–8

[28] Zhang D, Chippada U and Jordan K 2007 Effect of the structural water on the mechanical properties of collagen-like microfibrils: a molecular dynamics study *Ann. Biomed. Eng.* **35** 1216–30

[29] Radmer R J and Klein T E 2006 Triple helical structure and stabilization of collagen-like molecules with 4(R)-hydroxyproline in the Xaa position *Biophys. J.* **90** 578–88

[30] Bhowmik R, Katti K S, Verma D and Katti D R 2007 Probing molecular interactions in bone biomaterials: through molecular dynamics and Fourier transform infrared spectroscopy *Mater. Sci. Eng.* **27** 352–71

[31] Tomar V and Zhou M 2007 Analyses of tensile deformation of nanocrystalline α-Fe_2O_3 + fcc-Al composites using classical molecular dynamics *J. Mech. Phys. Solids* **55** 1053–85

[32] Orgel J, Irving T C, Miller A and Wess T J 2006 Microfibrillar structure of type I collagen *in situ Proc. Natl Acad. Sci. USA* **103** 9001–5

[33] Huang C C, Couch G S, Pettersen E F and Ferrin T E 1998 The object technology framework (OTF): an object-oriented interface to molecular data and its application to collagen *Pacific Symp. on Biocomputing* pp 349–60

[34] Phillips J C, Braun R, Wang W, Gumbart J, Tajkhorshid E, Villa E, Chipot C and Skeel R D 2005 Scalable molecular dynamics with NAMD *J. Comput. Chem.* **26** 1781–802

[35] Elliott J C, Mackie P E and Young R A 1973 Monoclinic hydroxyapatite *Science* **180** 1055–7

[36] Hein J, Reid F, Smith L, Bush I, Guest M and Sherwood P 2005 On the performance of molecular dynamics applications on current high-end systems *Phil. Trans. R. Soc.* **363** 1987–98

[37] Ponder J W and Case D A 2003 Force fields for protein simulations *Protein Simulations* (San Diego, CA: Academic) p 27

[38] Hauptmann S, Dufner H, Brickmann J, Kast S M and Berry R S 2003 Potential energy function for apatites *Phys. Chem. Chem. Phys.* **5** 635–9

[39] Bhowmik R, Katti K S and Katti D 2007 Molecular dynamics simulation of hydroxyapatite–polyacrylic acid interface *Polymer* **48** 664–74

[40] MacKerell A D, Bashford D, Bellott M, Dunbrack R L, Evanseck J D, Field M J, Fischer S, Gao J, Guo H, Ha S, Joseph-McCarthy D, Kuchnir L, Kuczera K, Lau F T K, Mattos C, Michnick S, Ngo T, Nguyen D T, Prodhom B, Reiher W E, Roux B, Schlenkrich M, Smith J C, Stote R, Straub J, Watanabe M, Wiorkiewicz-Kuczera J, Yin D and Karplus M 1998 All-atom empirical potential for molecular modeling and dynamics studies of proteins *J. Phys. Chem.* B **102** 3586–616

[41] Jorgensen W L, Chandrasekhar J, Madura J D, Impey R W and Klein M L 1983 Comparison of simple potential functions for simulating liquid water *J. Chem. Phys.* **79** 926–35

[42] Berg R A and Prockop D J 1973 The thermal transition of a non-hydroxylated form of collagen. Evidence for a role for hydroxyproline in stabilizing the triple-helix of collagen *Biochem. Biophys. Res. Commun.* **52** 115–20

[43] Holmgren S K, Taylor K M, Bretscher L E and Raines R T 1998 Code for collagen's stability deciphered *Nature* **392** 666–7

[44] Jenkins C L, Bretscher L E, Guzei I A and Raines R T 2003 Effect of 3-hydroxyproline residues on collagen stability *J. Am. Chem. Soc.* **125** 6422–7

[45] Park S, Radmer R J, Klein T E and Pande V S 2005 A new set of molecular mechanics parameters for hydroxyproline and its use in molecular dynamics simulations of collagen-like peptides *J. Comput. Chem.* **26** 1612–6

[46] Anderson D 2005 Collagen self-assembly: a complementary experimental and theoretical perspective *PhD Dissertation* University of Toronto

[47] Makarov V, Pettitt B M and Feig M 2002 Solvation and hydration of proteins and nucleic acids: a theoretical view of simulations and experiment *Acc. Chem. Res.* **35** 376–84

[48] Voth G A 2006 Computer simulation of proton solvation and transport in aqueous and biomolecular systems *Acc. Chem. Res.* **39** 143–50

[49] Posner A S and Beebe R A 1975 The surface chemistry of bone mineral and related calcium phosphates *Sem. Arthritis Rheum.* **4** 267–91

[50] Thompson J B, Kindt J H, Drake B, Hansma H G, Morse D E and Hansma P K 2001 Bone indentation recovery time correlates with bond reforming time *Nature* **414** 773–6

[51] Berryman J G 2005 Bounds and self-consistent estimates for elastic constants of random polycrystals with hexagonal, trigonal, and tetragonal symmetries *J. Mech. Phys. Solids* **53** 2141–73

[52] Broedling N C, Hartmaier A, Buehler M and Gao H 2008 The strength limit in a bio-inspired metallic nanocomposite *J. Mech. Phys. Solids* **56** 1086–104

[53] Chen J, Li L, Yu T, Long H, Weidner D, Wang L and Vaughan M 2006 Do Reuss and Voigt bounds really bound in high-pressure rheology experiments *J. Phys.: Condens. Matter* **18** S1049–59

[54] Rubin M A, Jasiuk L, Taylor J, Rubin J, Ganey T and Apkarian R P 2003 TEM analysis of the nanostructure of normal and osteoporotic human trabecular bone *Bone* **33** 270–82

[55] Simone A D, Vitaglaino L and Berisio R 2008 Role of hydration in collagen triple helix stabilization *Biochem. Biophys. Res. Commun.* **372** 121–5

[56] Bhowmik R, Katti K S and Katti D R 2007 Investigating the interfacial interactions between organic and inorganic phases and their influence on the mechanics of organic phase in natural bone *Mater. Res. Soc. Symp. Proc.* **975** 0975-DD02-05

[57] Ghosh P, Katti D R and Katti K S 2007 Mineral proximity influences mechanical response of proteins in biological mineral-protein hybrid systems *Biomacromolecules* **8** 851–6

[58] Keaveny T M, Morgan E F, Niebur G L and Yeh O C 2001 Biomechanics of trabecular bone *Annu. Rev. Biomed. Eng.* **3** 307–33